ELSEVIER

PII: S0032-3861(97)10092-1

Polymer Vol. 39 No. 17, pp. 3893–3900, 1998

0032-3861/98/$19.00+0.00

Influence of transreaction processes on the morphology of semicrystalline aliphatic/aromatic polyamide blends

K.L.L. Eersels[a], G. Groeninckx[a,*], M.H.J. Koch[b] and H. Reynaers[a]

[a]*Department of Chemistry, Laboratory for Macromolecular Structural Chemistry, Catholic University of Leuven, Celestijnenlaan 200F, B-3001 Heverlee-Leuven, Belgium*

[b]*European Molecular Biology Laboratory, EMBL c/o DESY, D-22603 Hamburg, Germany*

(Received 29 April 1997; accepted 2 September 1997)

During the melt-extrusion of blends of aliphatic polyamide 46 (PA 46) and aromatic polyamide 6I (PA 6I), transamidation reactions occur between the blend components. This yields polyamide copolymers consisting of crystallisable PA 46 and noncrystallisable PA 6I sequences. The effect of the copolymer formation on the semicrystalline morphology is studied by time-resolved SAXS and WAXS measurements using synchrotron radiation and by transmission electron microscopy. From WAXS patterns it is noticed that only an excess of PA 6I in the blends affects the PA 46 crystal unit cell at room temperature by hindering or inhibiting the Brill-transition during cooling from the melt. Close to the melting or crystallisation point, the PA 46 crystal structure is independent of the blend composition or thermal history. Consequently, the observed melting point depression cannot be ascribed to less perfect PA 46 crystals, but to a smaller lamellar thickness of the crystallised PA 46 sequences which is confirmed by TEM.

(Keywords: polyamide blends; transreaction; reactive extrusion)

INTRODUCTION

Melt-mixing of polycondensates results in transreaction processes between the blend components[1–9]. This phenomenon has often been used to obtain a finer phase dispersion during melt-processing of an initially immiscible blend system. Sometimes, even complete compatibility has been obtained by melt-mixing of two initial immiscible and non-compatible polycondensates[10–12]. This can be ascribed to the formation of block copolymers during the melt-mixing process. These copolymers, composed of the blend components, will decrease the interfacial tension between the separated phases and enhance compatibility.

The implications of reactive melt-blending of PA 46 with PA 6I on the molecular structure of the resulting copolyamides and on their thermal properties have been described previously[13–17]. It is, however, also important to assess the influence of the chain microstructure of the copolyamides on the development of the semicrystalline morphology during crystallisation of the PA 46 sequences from the melt to obtain fundamental information on the thermal properties of the PA 46/PA 6I copolyamides resulting from melt-blending.

It has been reported earlier that the melting temperature of the PA 46 crystals in the blends decreases as a function of the extrusion temperature and extrusion time[13]. Several authors have explained the pronounced melting point depressions by assuming that transreaction processes between polycondensates result in the formation of smaller and less perfect crystals during crystallisation[1,3,10]. A detailed study of the influence of the transreaction processes on the semicrystalline morphology is, however, not yet available.

* To whom correspondence should be addressed

Below we present a comprehensive investigation of the changes in the semicrystalline morphology of PA 46/PA 6I blends as a function of blend composition, melt-mixing and crystallisation conditions. This study was mainly performed by means of simultaneous time-resolved wide-angle (WAXS) and small-angle (SAXS) X-ray scattering using synchrotron radiation. The SAXS-results were compared with transmission electron microscopy data (TEM).

EXPERIMENTAL

Blend materials

As blend components PA 46 (DSM, $M_n = 20\,700$, $M_w = 51\,000$), a condensation product of 1,4-diaminobutane and adipic acid, and PA 6I (Bayer, $M_n = 8800$, $M_w = 28\,900$), a condensation product of 1,6-diaminohexane and isophthalic acid, were used.

Blend preparation

Prior to the melt-blending operation, PA 46 and PA 6I pellets were dried at 100°C under vacuum for at least 48 h. The DSM mini-extruder[13], was used to vary the extrusion time and temperature. Oxidative degradation was minimised by a nitrogen flow.

Several blend compositions of PA 46 and PA 6I were compounded using a ZSK 25 twin-screw extruder. The temperature of the melt was 315°C and the average residence time in the extruder, as determined by means of a master-batch, was about 2.5 min. The compounded blends were subsequently injection moulded into bars on a Battenfield injection machine. The melt-residence time during this process was about 1.5 min.

Real-time SAXS and WAXS measurements

Time-resolved simultaneous SAXS and WAXS

experiments were carried out on the double focusing monochromator-mirror camera X33 of the EMBL in HASYLAB on the storage ring DORIS III of the Deutsches Electronen Synchrotron (DESY) in Hamburg. Samples about 1 mm thick were sealed between thin (70 μm) aluminum foils and placed in a Mettler FP-82 HT oven used to control the thermal treatments during the X-ray scattering experiments. During these experiments the injection-moulded samples were heated at 10°C/min from room temperature to 300°C, where they were kept for 1 min and then cooled to 50°C at 10°C/min. The crystallised blends were subsequently heated to 300°C at 10°C/min. X-ray scattering patterns were recorded every 15 s, corresponding to a temperature increment of 2.5°C. They covered the range of scattering vectors of 3×10^{-3} s 2.5 10^{-2} Å in the SAXS range and 0.12 s 0.4 $Å^{-1}$ in the WAXS range; $s = 2 \sin \Theta/\lambda$, where 2Θ is the scattering angle and $\lambda = 1.5$ Å the wavelength.

The data were processed using the OTOKO software package[18].

Transmission electron microscopy

The blend materials were trimmed at room temperature and stained with a 50/50 solution of OsO_4/formaldehyde for 48 h. Thin sections (70 nm) were cut and investigated using a Philips CM200 Transmission Electron Microscope operated at 120 kV.

RESULTS AND DISCUSSION

Semicrystalline morphology of melt-processed PA 46/PA 6I blends

As the thermal properties of the PA 46/PA 6I blends are related to their semicrystalline morphology, it is useful to explore the ordering of the crystallised PA 46 component as well as the amorphous-crystalline supermolecular ordering. WAXS is suitable for the investigation of the crystallinity at the crystallite level. The difference in electron density between the two phases allows to gain information on the mutual ordering of the crystalline and amorphous regions in the semicrystalline blends by SAXS and TEM.

Time-resolved wide-angle X-ray scattering (WAXS)

Semicrystalline polyamides can exhibit polymorphism at room temperature; both monoclinic and/or triclinic lattices reflecting different chain alignment and stacking of hydrogen-bonded sheets can be obtained[19,20]. These structures are often indicated as α-structures. However, heating the polyamides to higher temperatures can result in a change of the crystalline lattice; the stable α-structure transforms into an unstable pseudo hexagonal γ-structure[21].

Crystal unit cell changes in polyamides as a function of temperature have already been reported earlier[22–24]. The solid-state transition from one type of crystal lattice to another as a function of temperature is known as the Brill-transition (T_b). This transition is believed to be related to a temperature-dependent chain packing[21]. At high temperatures, the vibration of the CH_2 groups with respect to the chain axis may result in a broadening of the spacing between the hydrogen-bonded sheets[22]. Possible reasons for the change of the unit cell as a function of the temperature include anisotropic thermal expansion[25] or the development of a three-dimensional network of hydrogen bonds between the chains[26,27]. Here, the crystalline chain segments are supposed to perform rotational jumps of 60° around their long axes, breaking the hydrogen bonds in the initial hydrogen-bonded sheet and making new ones with the molecules in the neighbouring sheet. This mechanism is known as the 60° flip-flop motion[28].

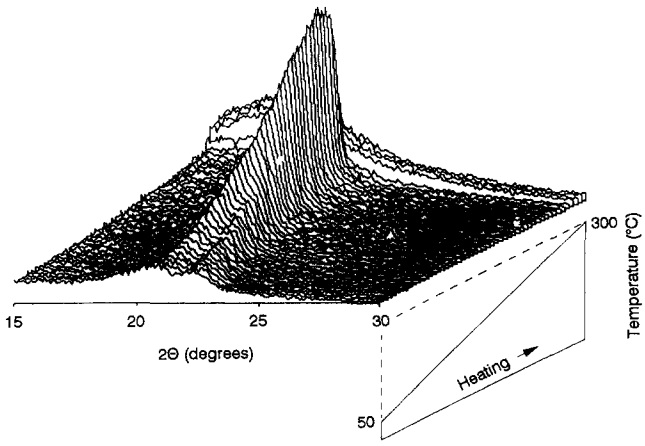

Figure 1 Evolution of the WAXS-patterns of PA 46 upon heating from 50 to 300°C at 10°C/min

The Brill-transition is observed when PA 46 is heated from room temperature into the melting region (*Figure 1*). The two strongest reflections of the α-structure, which is monoclinic and/or triclinic at 50°C, can be ascribed to the $d_{(100)}$ and the $d_{(110/010)}$ spacings. The separation between these reflections clearly becomes smaller with increasing temperature and they merge into a single reflection at the Brill-temperature. This implies that the $d_{(100)}$ and the $d_{(110/010)}$ spacings become equal and that a pseudohexagonal unit cell is formed.

The corresponding lattice spacings of PA 46 are given in *Figure 2a* as a function of the temperature during heating from 50 to 300°C. It can be seen that the $d_{(100)}$ spacing, which is mainly dominated by hydrogen bonds, slightly increases above 180°C as a result of anisotropic thermal expansion. However, the $d_{(110/010)}$ spacings, which correspond to the distance between the hydrogen-bonded sheets, increase considerably and finally become equal to the $d_{(100)}$ spacing at ~165°C. It is this pseudohexagonal crystal structure which ultimately melts at T_m.

It is obvious from these observations that the melting behaviour of polyamides cannot be related to the low-temperature α-structures, but must be related to the high-temperature pseudohexagonal γ-structures just before melting.

Similar phenomena are observed when PA 46 is cooled from the melt, as shown in *Figure 2b*. Crystallisation will occur in the pseudohexagonal γ-form which transforms into the more stable α-structure below the Brill-temperature.

The impact on the crystal lattice of PA 46 of melt-mixing PA 46 with an amorphous aromatic PA 6I is of special interest. The copolyamides formed during reactive melt-blending, are composed of crystallisable and non-crystallisable sequences. In *Figure 3a*, the lattice spacings of different blends crystallised by cooling from the melt at − 10°C/min are given as a function of temperature. All blend compositions crystallise in the pseudohexagonal form from where they transform into the more stable α-form below the Brill-temperature. As shown in *Table 1*, the Brill-transition temperature during cooling from the melt ($T_{b,c}$) is lower for the blend containing 70% PA 6I. *Figure 3a* also illustrates that the splitting of the (100) and (010/110) reflections of the 70% PA 6I blend is less pronounced. The blend composed

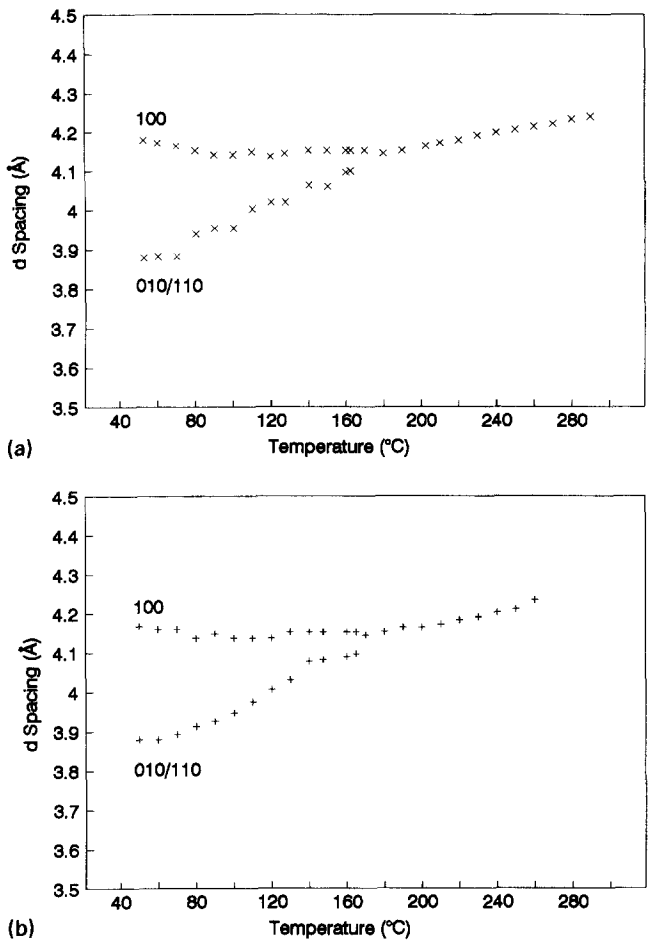

Figure 2 (a) Temperature dependence of the lattice spacings, $d_{(100)}$ and $d_{(110/010)}$, of PA 46 upon heating from 50 to 300°C at 10°C/min. (b) Temperature dependence of the lattice spacings, $d_{(100)}$ and $d_{(110/010)}$, of PA 46 upon cooling from 300 to 50°C at 10°C/min

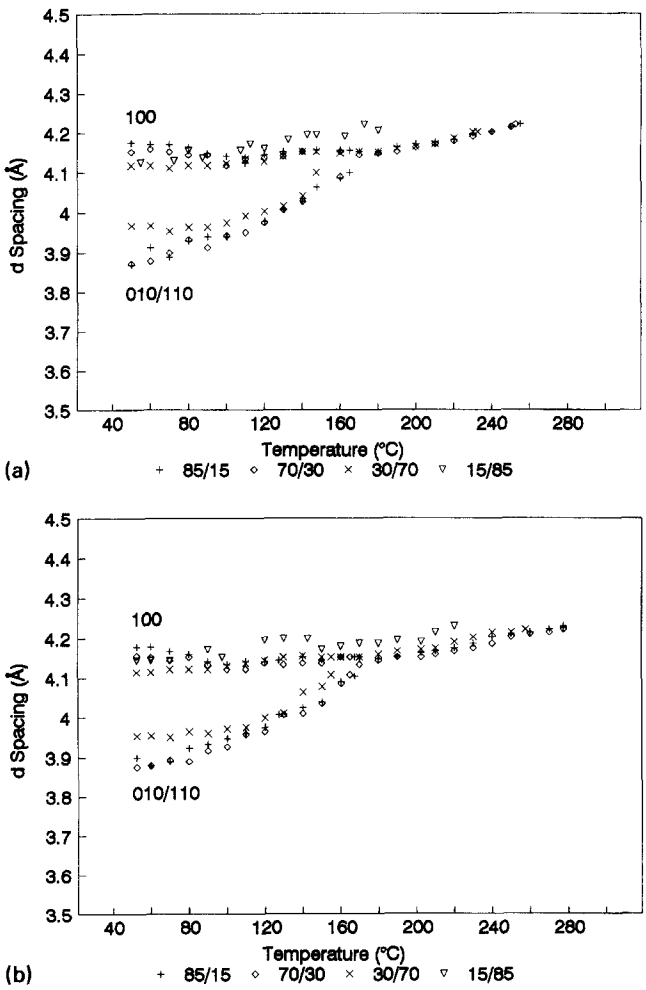

Figure 3 (a) Temperature dependence of the lattice spacings, $d_{(100)}$ and $d_{(110/010)}$, of PA 46/PA 6I blends upon cooling from 300 to 50°C at 10°C/min. Blend compositions (PA 46/PA 6I): (+) 85/15; (◇) 70/30; (×) 30/70; (▽) 15/85. (b) Temperature dependence of the lattice spacings, $d_{(100)}$ and $d_{(110/010)}$, of PA 46/PA 6I blends upon heating from 50 to 300°C at 10°C/min. Blend compositions (PA 46/PA 6I): (+) 85/15; (◇) 70/30; (×) 30/70; (▽) 15/85

Table 1 Influence of the PA 46/PA 6I blend composition on the crystallization peak temperature T_c, the melting peak temperature T_m and the Brill-transition temperature during cooling from the melt ($T_{b,c}$) and during reheating ($T_{b,h}$): scanning rate, 10°C/min

Blend composition (PA 46/PA 6I)	T_c (°C)[a]	$T_{b,c}$ (°C)	T_m (°C)[a]	$T_{b,h}$ (°C)
100/0	262	165 ± 2.5	292	165 ± 2.5
85/15	259	165	290	170
70/30	256	160	287	165
30/70	238	150	272	155
15/85	203		254	

[a]Values obtained by d.s.c.

of 15% PA 46 and 85% PA 6I does not show a Brill-transition and remains mainly in the pseudohexagonal form, even at lower temperatures. High concentrations of amorphous PA 6I in the blend clearly hinder the pseudohexagonal to monoclinic/triclinic transformation of the PA 46 crystals, and a pseudohexagonal frozen-in structure is obtained at room temperature. Similar observations were made by Zimmerman *et al.*[29], who found that increasing the concentration of PA 2Me6T in melt-mixed blends with PA 66 inhibits the normal hexagonal to triclinic transition of PA 66.

The pseudohexagonal to monoclinic/triclinic transition is also hindered by increasing the cooling rate from the melt. This is illustrated by the WAXS pattern of injection moulded bars. It has been observed from the lattice spacings for the injection moulded samples (rapid cooling), as a function of the blend composition, that the splitting of the (100) and (110/010) reflections of PA 46 at 50°C is much less pronounced than in slowly cooled PA 46. The blend containing 30% PA 46 and 70% PA 6I remains in the pseudohexagonal form after injection moulding, and yields a frozen-in structure. The blend with 85% PA 6I only reveals an amorphous halo which indicates that crystallisation during injection moulding is inhibited.

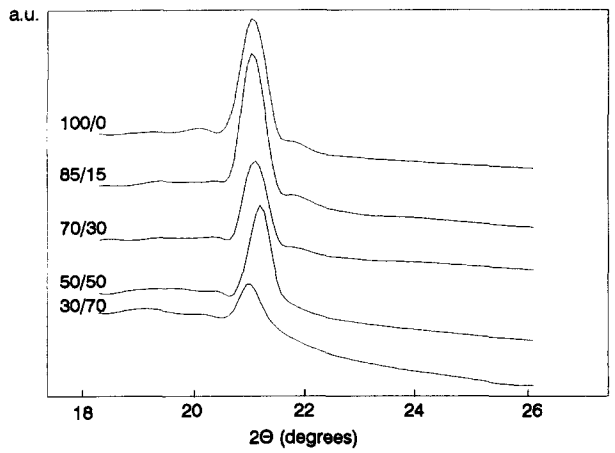

Figure 4 WAXS diffraction patterns of different PA 46/PA 6I blend compositions at 240°C. Blend compositions (PA 46/PA 6I): 100/0; 85/15; 70/30; 50/50; 30/70

Annealing of this blend at 200°C, however, results in cold-crystallisation.

The change of the lattice spacings of the slowly cooled blends during heating is represented in *Figure 3b*. The pseudohexagonal to monoclinic/triclinic transformation seems to be reversible. Notice that the crystal lattice parameters of the pseudohexagonal structures just before melting are independent of the blend composition. Moreover, the full width half maximum of the PA 46 reflections at 240°C of all blend compositions in *Figure 4* remains constant. The independence of both the lattice spacings and the peak width on blend composition suggests that the PA 6I units, which cannot be incorporated in the PA 46 crystals, do not affect the PA 46 crystal structure. Nevertheless, the melting temperature of PA 46 in the blends decreases with increasing PA 6I content (*Table 1*).

Figure 5a represents the $d_{(100)}$ and $d_{(110/010)}$ lattice spacings of a 50/50 blend, obtained after different melt-residence times, as a function of temperature during cooling from the melt. The change of the sequence lengths of the polyamide copolymers as a function of the melt-residence time has been studied previously in detail[15]. It was found that increasing the melt-mixing time increases the degree of randomness and decreases the block copolymer sequence lengths, giving rise to a lower crystallisation temperature of PA 46 in the blends. However, the melt-residence time does not seem to affect the lattice parameters of PA 46 just after crystallisation (*Figure 5a*). There is only a small increase of the $d_{(110/010)}$ spacings at lower temperatures with increasing melt-residence time which is paralleled by a decrease of the Brill-temperature (*Table 2*).

The evolution of the lattice spacings during heating and melting of the blends is shown in *Figure 5b*. The lattice spacings, just before melting, are independent of the melt-residence time, although the melting temperature sharply drops with increasing melt-residence time (*Table 2*).

Summarising, it can be concluded from the time-resolved WAXS measurements that the blend composition and the processing conditions affect the Brill-transition temperature and the lattice spacings at room temperature, but do not seem to influence the lattice parameters immediately after crystallisation or just before melting.

Time-resolved small-angle X-ray scattering (SAXS)

The amorphous/crystalline ordering in the blends can be studied by means of SAXS. The room temperature

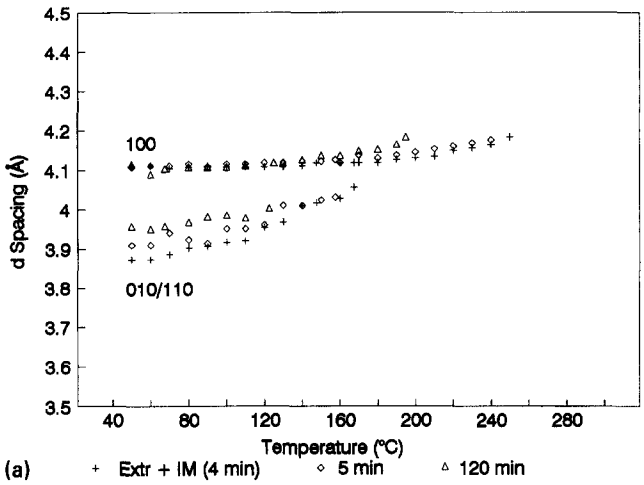

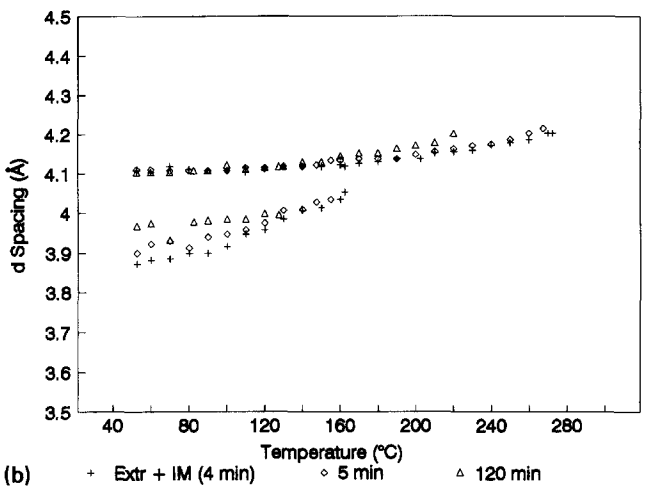

Figure 5 (a) Temperature dependence of the lattice spacings, $d_{(100)}$ and $d_{(110/010)}$, of the PA 46/PA 6I (50/50) blend upon cooling from 300 to 50°C at 10°C/min. Extrusion temperature, 315°C. Melt-residence time, +4 min (extruded plus IM); (◇) 5 min; (△) 120 min. (b) Temperature dependence of the lattice spacings, $d_{(100)}$ and $d_{(110/010)}$, of the PA 46/PA 6I (50/50) blend upon heating from 50 to 300°C at 10°C/min. Extrusion temperature, 315°C. Melt-residence time, + 4 min (extruded plus IM); (◇) 5 min; (△) 120 min

background-corrected and Lorentz-corrected SAXS patterns of the different PA 46/PA 6I blend compositions, cooled from the melt at 10°C/min, are given in *Figure 6a* and *b*, respectively.

The SAXS patterns reveal a broad maximum indicating a large distribution of the long period L. The total scattered intensity at small angles markedly decreases with increasing concentration of PA 6I in the blends. This decrease in scattered intensity can result from a combination of several factors. Assuming a two-phase system, the scattered intensity is related to the invariant $\langle\eta\rangle^2$, which depends on the degree of crystallinity ϕ and the difference in electron density between the crystalline phase (ρ_c) and the amorphous phase (ρ_a):

$$\langle\eta\rangle^2 \cong \phi(1-\phi)(\rho_c - \rho_a)^2 \qquad (1)$$

(i) The electron density of the amorphous phase ρ_a of the blend will increase with the amount of PA 6I in the amorphous phase, since the density of PA 6I (1.18 g/cm^3) is slightly higher than that of amorphous PA 46 (1.10 g/cm^3). Furthermore, it appears from the WAXS measurements that ρ_c of PA 46 does not depend on the blend composition for blends with 50 wt.% of PA 6I and less, and slightly decreases in blends containing 70 wt.% of PA 6I

Table 2 Influence of the melt-processing time on the crystallization peak temperature T_c, the melting peak temperature T_m and the Brill-transition temperature of PA 46/PA 6I (50/50) blends during cooling from the melt ($T_{b,c}$) and during reheating ($T_{b,m}$): cooling and heating rate, 10°C/min

Processing time (min)	T_c (°C)[a]	$T_{b,c}$ (°C)	T_m (°C)[a]	$T_{b,h}$ (°C)
4 (extruded + IM)	252	165 ± 2.5	282	165 ± 2.5
5	245	155	279	155
120	202	125	240	130

[a]Values obtained by d.s.c.

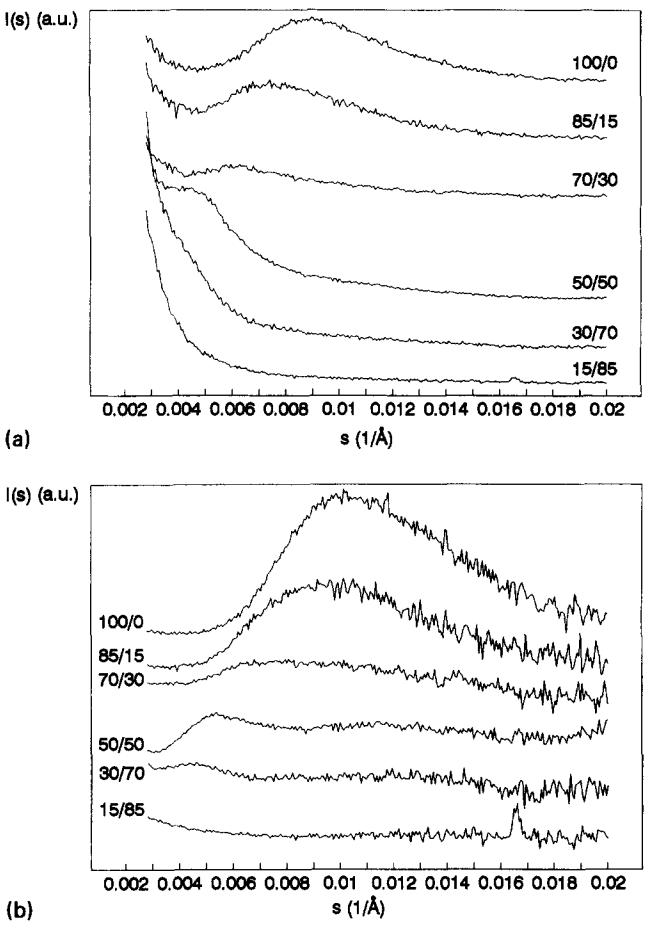

Figure 6 (a) Background subtracted SAXS curves of PA 46/PA 6I blends, cooled from the melt at 10°C/min, recorded at 25°C. (b) Lorentz corrected background subtracted SAXS curves of PA 46/PA 6I blends, cooled from the melt at 10°C/min, recorded at 25°C

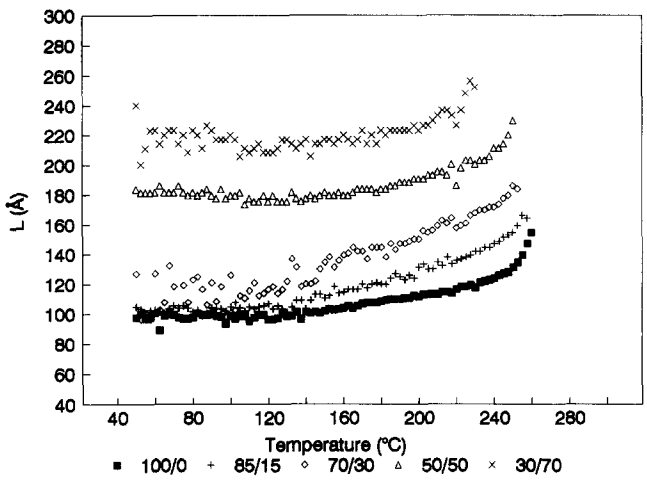

Figure 7 Variation of the long spacing L *versus* temperature for PA 46/PA 6I blends upon cooling from 300 to 50°C at 10°C/min. Blend compositions (PA 46/PA 6I): (■) 100/0; (+) 85/15; (◇) 70/30; (△) 50/50; (×) 30/70.

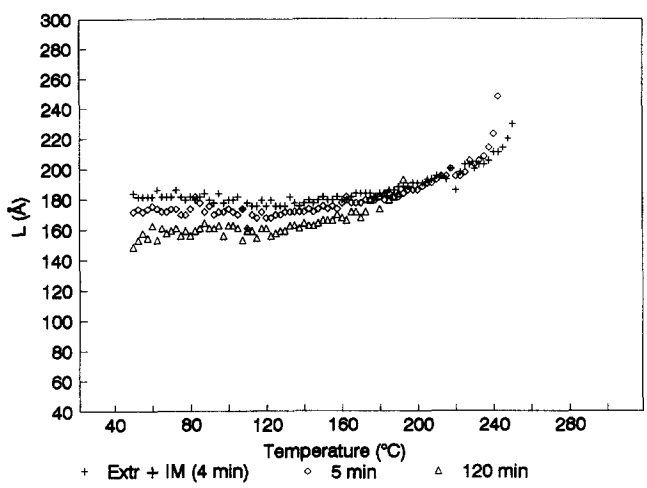

Figure 8 Variation of the long spacing L with temperature for the PA 46/PA 6I (50/50) blend upon cooling from 300 to 50°C at 10°C/min. Extrusion temperature, 315°C. Melt residence time, + 4 min (extruded plus IM); (◇) 5 min; (△) 120 min

and more. Consequently, $(\rho_c - \rho_a)^2$ decreases which will affect the scattered intensity.

(ii) A larger volume fraction of PA 6I in the blends will result in a decrease of the total degree of crystallinity ϕ. If $\phi < 50\%$, $\phi(1 - \phi)$ becomes smaller with decreasing blend crystallinity, and the invariant thus also decreases. However, $\phi(1 - \phi)$ changes only slightly when ϕ varies between 30 and 70%.

(iii) An additional cause for the decrease in scattered intensity could be, as illustrated by the TEM micrographs below, the decrease of stacking order of the crystalline lamellae of the PA 46 sequences when the PA 6I content in the blend is higher.

Figure 7 illustrates the large variations in the long spacing L as a function of blend composition. Increasing the weight content of PA 6I in the blends from 0 to 85%, increases the long spacing from about 100 to 230 Å, indicating segregation of PA 6I in the interlamellar amorphous regions of the blends.

Figure 8 represents the variation of the long spacing L *versus* temperature for the PA 46/PA 6I (50/50) blend with different melt-residence times after slow cooling from the melt. L decreases when the melt-residence time is increased, as was also observed when the extrusion temperature was increased. This can be ascribed to a reduction of the interlamellar amorphous thickness and/or the crystalline lamellar thickness.

Figure 9 indicates how the SAXS-pattern of pure PA 46 changes upon heating. The total scattered intensity increases at elevated temperatures because of an increasing difference between the crystalline density ρ_c and the amorphous

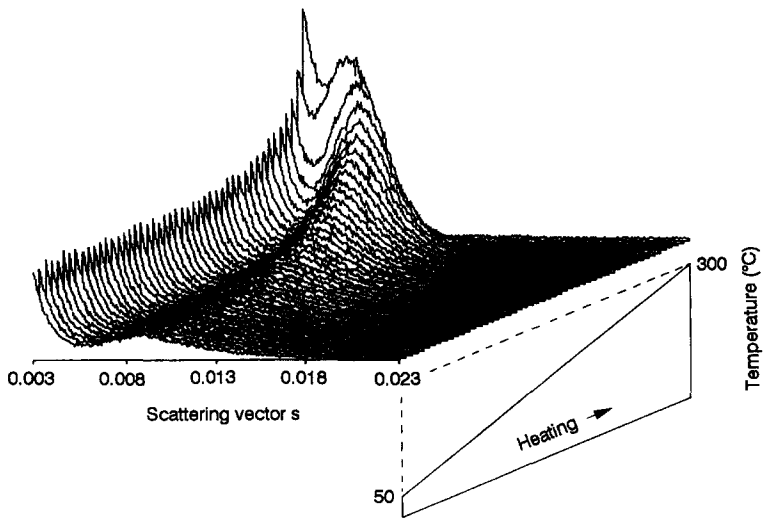

Figure 9 Evolution of the SAXS-pattern of PA 46 upon heating from 50 to 300°C at 10°C/min

density ρ_a. The shift of the diffraction peak to lower angles at high temperatures can be ascribed to the progressive melting of the least stable crystalline lamellae; such a melting mechanism results in an increase of the long spacing and the concomitant shift of the scattering maximum to lower angles. The scattering vanishes when all the lamellae are molten.

Transmission electron microscopy (TEM)

A better insight into the semicrystalline morphology of blends cooled from the melt at −10°C/min is obtained by combining SAXS and TEM observations. The lamellar structure of PA 46 is shown in *Figure 10a*. The densely packed lamellar morphology supports the interpretation of the SAXS analysis in terms of lamellar stacks. The least stained areas are the crystalline regions, while the heavily stained ones correspond to the amorphous phase. The crystalline lamellae have a thickness of about 30–40 Å. Adding 50% by weight of PA 6I results in the morphology shown in *Figure 10b*. The crystalline lamellae are covered by a heavily stained layer. Since pure PA 6I stained under comparable conditions yields bright micrographs, it can be concluded that the heavily stained layers along the crystalline lamellae represent mainly amorphous PA 46. The region between the crystalline lamellae consists of amorphous PA 6I and amorphous PA 46. The morphology of the blend composed of 30% PA 46 and 70% PA 6I is given in *Figure 10c*. The interlamellar spacings are larger and the crystalline lamellar thickness is estimated at 20–30 Å.

Relation between the crystalline morphology and the melting behaviour of the PA 46/PA 6I copolymers

The quantitative interpretation of the melting behaviour of the PA 46/PA 6I copolyamides formed during reactive melt-extrusion is very difficult because of the complexity of the structures formed. In the previous section, it was shown on the basis of the WAXS data that melt-mixing of PA 46 with PA 6I does not seem to have a substantial effect on the perfection of the PA 46 crystals at the onset of the melting. Although large melting point depressions have been observed as a function of the blend composition and the melt-processing conditions, the crystalline perfection of the pseudohexagonal structures just before melting remains unaffected regardless of the blend composition and the processing conditions.

SAXS measurements and TEM observations indicate a variation of the long-range stacking order with increasing weight content of PA 6I. Besides this loss of stacking order, TEM micrographs also reveal a small decrease of the crystalline thickness.

The relation between the crystalline lamellar thickness and the resulting melting temperature for semicrystalline homopolymers is described by the Hoffman–Weeks equation[30,31]:

$$T_m = T_m^0\left(1 - \frac{2\sigma_e}{l_c \Delta H_m^0}\right) \quad (2)$$

where T_m^0 is thermodynamic equilibrium melting temperature; l_c is crystalline lamellar thickness; σ_e is fold surface free energy; ΔH_m^0 is melting enthalpy of a perfect infinite crystal.

For PA 46, the lamellar thickness can be calculated from equation (2) knowing the observed melting temperature and using the following reference values[32]: $T_m^0 = 350$°C, $\sigma_e = 75 \times 10^{-3}$ J/m^2, $\Delta H_m^0 = 210$ J/g (251 J/cm^3). A lamellar thickness of 36 Å is obtained, which is within the range of lamellar thicknesses observed by TEM.

It can be derived from equation (2) that a small decrease in the crystalline lamellar thickness of PA 46, due to the reactive melt-mixing process with PA 6I, can cause large melting point depressions.

CONCLUSIONS

Melt-mixing of PA 46 and PA 6I results in the formation of copolymers consisting of crystallisable sequences of PA 46 and non-crystallisable sequences of PA 6I. The non-crystallisable sequences of PA 6I do not affect the crystal lattice parameters of PA 46 unless PA 6I is present in an excess. In the latter case, PA 6I hinders or inhibits the Brill-transition of the PA 46 crystals during cooling from the melt. The PA 46 crystal structure in the blends, just before the melting transition, appears to be independent of the blend composition and the melt-processing conditions and, consequently, cannot account for the observed melting point depressions. The latter can be ascribed to a decrease of the crystalline lamellar thickness of PA 46, as observed by TEM. TEM and SAXS measurements indicate that an excess of PA 6I in the blends results in a large increase of the long spacing when the blends are slowly cooled from the melt.

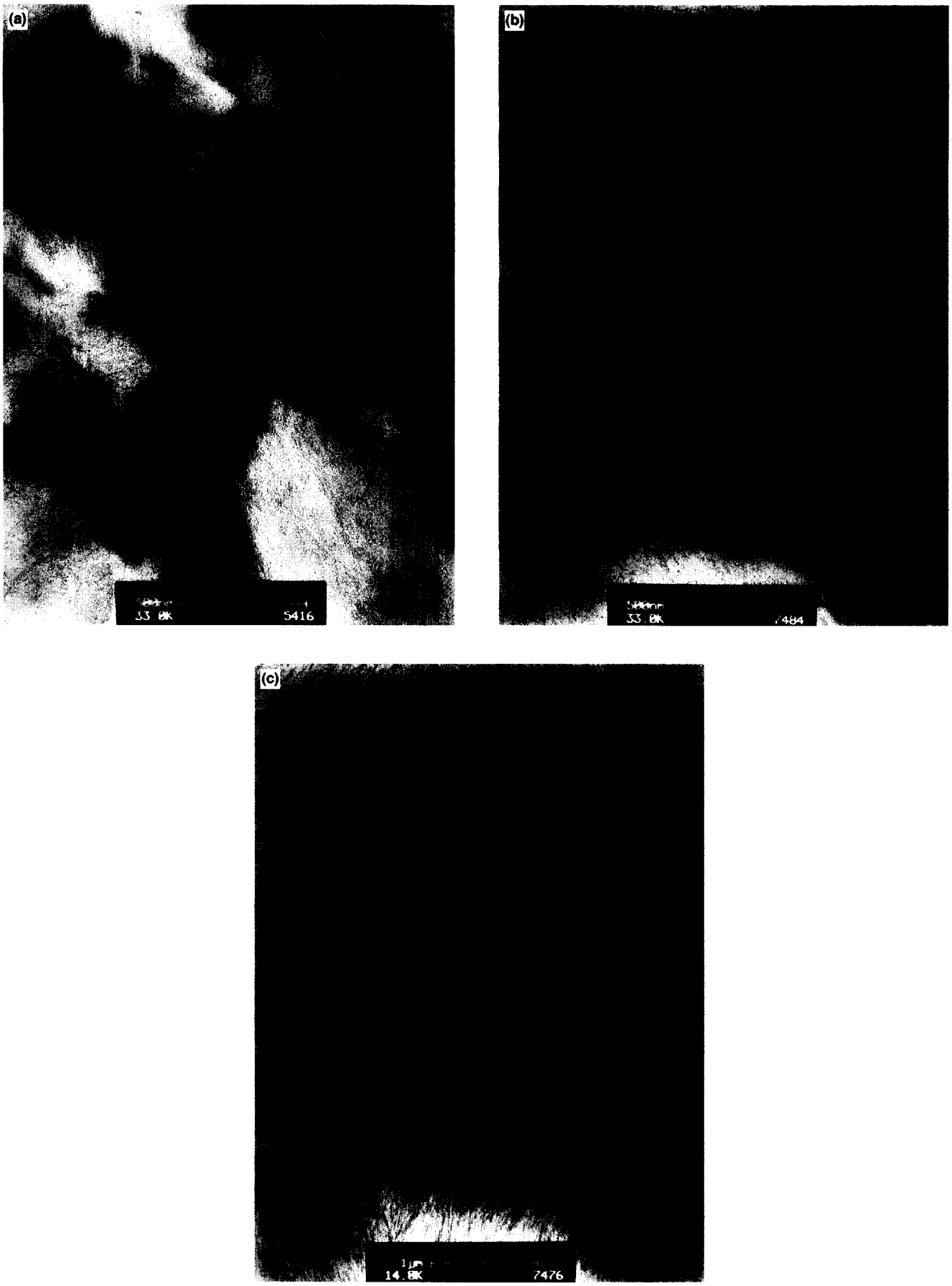

Figure 10 (a) Lamellar morphology of PA 46, slowly cooled from the melt; (b) lamellar morphology of PA 46/PA 6I (50/50) blend, slowly cooled from the melt; (c) lamellar morphology of PA 46/PA 6I (30/70) blend, slowly cooled from the melt

ACKNOWLEDGEMENTS

The authors would like to thank the European Union for support of the work at EMBL Hamburg through the HCMP to Large Installation Project, contract no. CHGE-CT93-0040. They are also indebted to Monique Walet and Yvonne Engelen (DSM Research, Geleen, The Netherlands) for taking the TEM micrographs and to Prof. A. Keller (University of Bristol, England) and Stephan Eltink (DSM Research) for valuable discussions. They also wish to express their appreciation to DSM Research, Geleen, The Netherlands, for financial support of this study.

REFERENCES

1. Martinez, J. M., Nazábal, J. and Eguiazábal, J. I., *J. Appl. Polym. Sci.*, 1994, **51**, 223.
2. Eguiazábal, J. I., Ucar, G., Cortázar, M. and Iruin, J. J., *Polymer*, 1986, **27**, 2013.
3. Kimura, M., Salee, G. and Porter, R. S., *J. Polym. Sci.; Polym. Phys. Ed.*, 1984, **29**, 1629.
4. Stewart, M. E., Cox, A. J. and Naylor, D. M., *Polymer*, 1993, **34**, 4060.
5. Gattiglia, E., Tarturro, A., Lamantia, F. P. and Valenza, A., *J. Appl. Polym. Sci.*, 1992, **46**, 1887.
6. Porter, R. S. and Li-Hui, Wang, *Polymer*, 1992, **33**, 2019.
7. Miley, D. M. and Runt, J., *Polymer*, 1992, **33**, 4643.
8. Devaux, J., Godard, P. and Mercier, J. P., *Polym. Eng. Sci.*, 1982, **22**, 229.
9. Kotliar, A. M., *J. Polym. Sci.; Macromol. Rev.*, 1981, **16**, 367.
10. Cortázar, M., Eguiazábal, J. I. and Iruin, J. J., *Eur. Polym. J.*, 1994, **30**, 901.
11. Takeda, Y. and Paul, D. R., *Polymer*, 1992, **33**, 3899.
12. Zheng, W-g., Qi, Z-n. and Wang, F-s., *Polym. Intern.*, 1994, **34**, 307.
13. Eersels, K. L. L. and Groeninckx, G., *Polymer*, 1996, **37**, 983.
14. Aerdts, A. M., Eersels, K. L. L. and Groeninckx, G., *Macromolecules*, 1996, **29**, 1041.
15. Eersels, K. L. L., Aerdts, A. M. and Groeninckx, G., *Macromolecules*, 1996, **29**, 1046.
16. Eersels, K. L. L., Groeninckx, G., Mengerinck, Y. and van der Wal, Sj., *Macromolecules*, 1996, **29**, 6744.
17. Eersels, K. L. L. and Groeninckx, G., *J. Appl. Polym. Sci.*, 1997, **63**, 573.
18. Boulin, C., Kempf, R., Koch, M. H. J. and McLaughlin, S. M., *Nucl. Instruments Methods*, 1986, **A249**, 399.
19. Parker, J. P. and Lindenmeyer, P. H., *J. Appl. Polym. Sci.*, 1977, **21**, 821.
20. Gaymans, R. J., Doeksen, D. K. and Harkema, S., *Integration of Fundamental Polymer Science and Technology*, Volume I, ed. L. Kleintjens, L. and P. Lemstra. Elsevier, Amsterdam, 1986, p. 573.
21. Brill, R., *J. Prakt. Chem.*, 1942, **161**, 49.
22. Itoh, T., *Jap. J. Appl. Phys.*, 1976, **15**, 2295.
23. Ramesh, C., Keller, A. and Eltink, S. J. E. A., *Polymer*, 1994, **35**, 2483.
24. Atkins, E. D. T., *J. Macromol. Sci.; Pure Appl. Chem.*, 1994, **A31**, 691.
25. Holmes, D. R., Bunn, C. W. and Smith, D. J., *J. Polym. Sci.*, 1955, **17**, 159.
26. Brill, R., *Makromol. Chem.*, 1956, **18**, 2940.
27. Schmidt, G. F. and Stuart, H. A., *Z. Naturforsch.*, 1958, **13a**, 222.
28. Olf, H. G. and Peterlin, A., *J. Polym. Sci., A-2*, 1971, **9**, 1449.
29. Zimmerman, J., Pearce, E. M., Miller, I. K., Muzzio, J. A., Epstein, I. G. and Hosewood, E. A., *J. Appl. Polym. Sci.*, 1973, **17**, 849.
30. Wunderlich, B., *Macromolecular Physics*, Vol. 3, *Crystal Melting*. Academic Press, New York, 1980.
31. Hoffman, J. D. and Weeks, J. J., *J. Res. Nat. Bur. Stand. (A)*, 1962, **66**, 13.
32. Derks, W. H. P., Moonen, J. A. H. M., Ramaekers, F. J. W. and Kooij, C. J., *IUPAC Conference*, Abstracts, Montréal, Canada, 1989.